

## Chapter 3

# Fast Metabolic Response to Drug Intervention through Analysis on a Miniaturized, Highly Integrated Molecular Imaging System

### 3.1. Introduction

*In vivo* molecular imaging assays, employing a variety of probes of specific biological processes, have been developed for positron emission tomography (PET). The most common probe in patients care and research is the glucose analog, 2-deoxy-2- $[^{18}\text{F}]$ fluoro-deoxy-D-glucose ( $[^{18}\text{F}]$ FDG) for imaging and measuring rates of glycolysis. In cancer patients,  $[^{18}\text{F}]$ FDG assays are used for diagnosis and assessing therapeutic responses<sup>1</sup>. Around 3,000 molecular imaging probes for PET have been reported for various metabolic and other processes associated with disease states<sup>1</sup>.

*In vitro* metabolic assays using radio-labeled probes have been adapted to 96-well plates and microchip formats<sup>2</sup>. We explore here the use of such assays for quantitating the kinetics of cellular responses to targeted drugs. We first introduce a microfluidic chip design (the RIMChip) that couples to a beta-particle imaging camera<sup>2-4</sup> to form the betabox. The betabox is designed for the quantitative analysis of the metabolic response of small numbers of cells to pharmaceuticals. Most assay steps are similar to those of standard 96-well plate radioassays, but require far fewer cells, permit quantitation of signal per cell, and utilize live cells. The platform is validated on various adherent and suspension cancer cells. We characterize the influence of the monocarboxylate transporter (MCT1) protein, as well as a glycolytic inhibitor, on  $[^{18}\text{F}]$ FDG uptake in isogenic

liposarcoma cells. Using different liposarcoma cells, we investigate the influence of deoxycytidine kinase (dCK)<sup>5</sup> on the uptake of the deoxycytidine analog molecular imaging probe [<sup>18</sup>F]-FAC<sup>6</sup>.

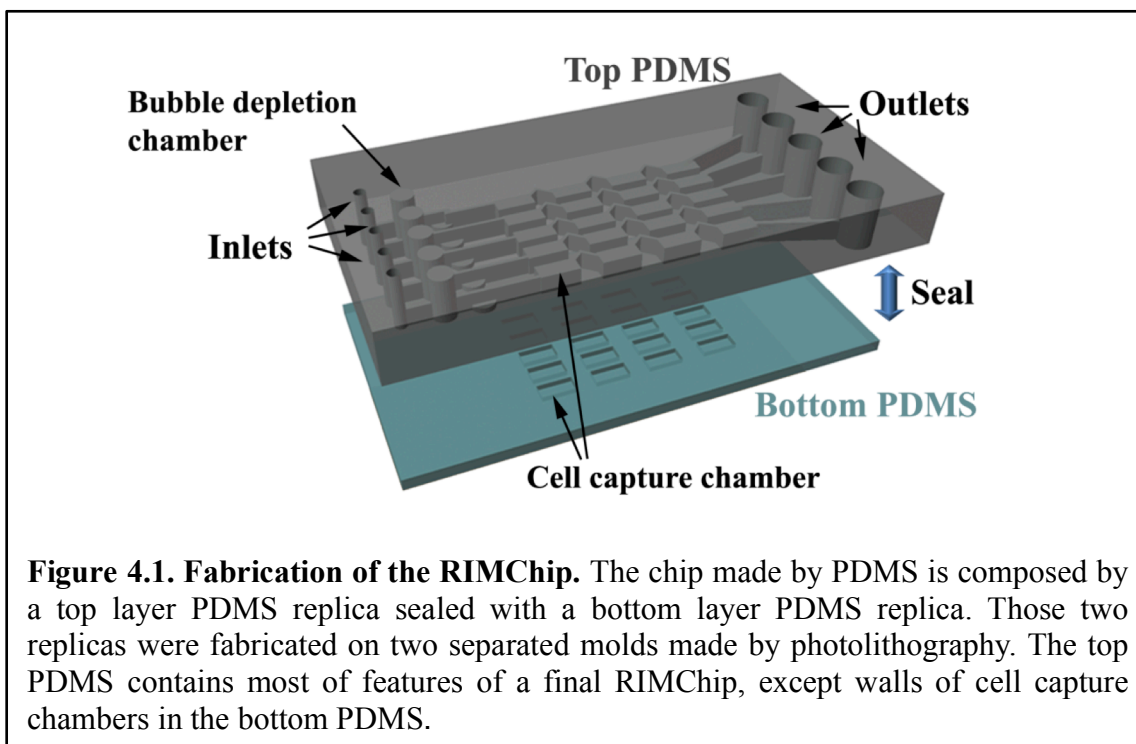
We then explore how certain cancer cell lines respond to two mechanistically distinct targeted inhibitors. We quantitate the response kinetics of liposarcoma cells to gemcitabine<sup>7</sup> by correlating cell-cycle arrest with [<sup>18</sup>F]FDG uptake. We then quantitate the kinetic response of model glioblastoma multiforme (GBM) cancer cells to an epidermal growth factor receptor (EGFR) inhibitor, by correlating changes in [<sup>18</sup>F]FDG uptake with the levels of phosphoproteins associated with EGFR signaling. Glucose consumption consistently provides a rapid (~ 30 min.) indicator of positive therapeutic response, and the betabox platform provides a simple tool for quantitating those kinetics.

## **3.2. Experimental Methods**

### **3.2.1. RIMChip design concepts**

The RIMChip design has 5 microchannels for executing 5 distinct assay conditions. Each microchannel has 4 microchambers in which the assays are executed, and so a single assay condition is repeated four times. Several key features are designed into each microchannel to ease the execution of processes such as imaging, cell loading, and reagent flushing and delivery. First, the spatial resolution of the beta camera is 600  $\mu\text{m}$ , and nearest edges of neighboring microchambers are separated by 800  $\mu\text{m}$  to avoid signal overlap (**Fig. 3.1.**). Second, the microchannels are designed so that cells are only captured within the microchambers. An individual cell chamber contains a 7 $\times$ 3 waffle-structured

array of 200  $\mu\text{m}$  deep microwells, separated by 30  $\mu\text{m}$  thick walls. This structure is designed to minimize the shear stress exerted onto cells that are attached to the bottom of microwells when flushing through new medium or reagents. This waffle design also helps maintain the rigidity of the bottom surface. Third, this bottom surface is only 50  $\mu\text{m}$  thick due to the constraint that the assay sensitivity depends upon the proximity of the cells to the camera. This thin-floored PDMS chip provides a  $\sim 130\%$  increase in collected signal over a common glass microscope coverslip. It also means that cells that do get trapped in places away from the microchambers do not provide detectable signal during an assay, since those cells will have up to 1 mm of PDMS separating them and the beta camera. Fourth, the microchannel inlet is designed to avoid clogging of the channels by either bubbles, clumps of cells, or other debris, and for ease of use. The microchannel inlets accommodate a 20-200  $\mu\text{l}$  pipette tip so that standard microwell procedures may be used. The bubble depletion chamber has a volume of 0.95  $\mu\text{l}$ , and successfully removes any bubbles that are introduced in the micropipetting steps. The bubble depletion volume is followed by a filtering area of posts that have a tailored depth of between 25 and 35  $\mu\text{m}$ . This dimension is customized for specific cell-types. In this study, we designed a 32  $\mu\text{m}$  gap for liposarcoma cell lines and the U87 isogenic cell lines, and 20  $\mu\text{m}$  gap for all suspended cells (which have a smaller cell size). The filter design also significantly enhances the hydrodynamic resistance of a channel and prevents backflow at the completion of solution injection. This means that cell loading uniformity is significantly increased. The outlet volume of the microchip holds all of the overflow from a given micropipetting step, and that overflow is removed using a micropipette. The microchamber area of the RIMChip area has a 1 cm  $\times$  1 cm footprint, and which is designed to match the beta-particle camera.



### 3.2.2. RIMChip fabrication

The microchip is fabricated from multiple layers of the elastomer polydimethylsiloxane (PDMS) using standard soft lithography methods as previously described<sup>3</sup>. PDMS is air permeable, which is helpful for both removing bubbles through the bubble depletion chamber, and also for assisting in on-chip cell incubation. The filter layer was patterned on a 4" silicon wafer, using negative photoresist SU8 2025 (Microchem). On the same wafer, the fabrication of a layer of SU8 2100 generated the microchannel features that mate to the filters. This layer has a depth of 200  $\mu\text{m}$ , which is also the microchannel depth. This ensures a sufficient nutrition supply to allow several hours of on-chip cell incubation. The cell chamber features were patterned using SU8 2025 on a separate wafer. Those two masters were used to mold the PDMS. Precure PDMS mixture at the ratio of 5:1

was poured onto the master with the microchannel and filter layers, and baked at 80 °C for 1 h to cure the PDMS (top PDMS in **Fig. 3.1.**). Meanwhile another PDMS precure mixture at the ratio of 20:1 was molded on to the second master. This PDMS replica was peeled off from this master, flipped and laid flat on a clean wafer (bottom PDMS in **Fig. 3.1.**). The top PDMS and the bottom PDMS layers were then trimmed and punched with appropriate inlet and outlet holes at 1.5 mm and 5 mm diameters, respectively, and then aligned and mated. The microchip was baked at 80 °C overnight to seal the PDMS layers. Finally, the entire microchannel was filled with PBS solution through dead-end filling by exerting 3 psi N<sub>2</sub> pressure in a tubing connected to the microchip

### **3.2.3. The beta-particle camera (Betabox)**

The Betabox is a direct detection beta-particle detection camera utilizing a 13.5 x 13.5 mm<sup>2</sup> active area position sensitive avalanche photodiode (PSAPD) (Radiation Monitoring Devices). The five outputs of the PSAPD first pass through CR-110 charge sensitive preamplifiers and then shaping amplifiers with a 200 ns shaping time. The shaped sum signal then passes to a threshold comparator which produces event trigger pulses to four sample and hold (S/H) circuits (53ns acquisition time, 6μs hold time) to initiate an analog to digital conversion of the positioning channels using a simultaneous sampling data acquisition system (DAQ) (National Instruments PCI-6143).

### **3.2.4. Cell sample preparation, viability, and cell-cycle assays**

Liposarcoma cell lines LPS1 and LPS2 with dCK- and MCT1-knockdown, respectively, were derived from patient samples. Lentiviral-based, shRNA-mediated

knockdown of MCT1 and dCK were described in the previous literature<sup>8</sup>, The murine leukemic lines (L1210 wt and L1210-10K)<sup>9</sup> were a kind gift from Charles Dumontet (Université Claude Bernard Lyon I, Lyon, France)<sup>10</sup>. The human lymphoma line CEM was purchased from ATCC (#CCL-119) and the sub-line, CEM-dCK negative, was generated via selection with ara-C<sup>11</sup> and was a gift of Margaret Black (Washington State University). A human leukemia T cell line (Jurkat T) was purchased from ATCC. The human glioblastoma cell line U87 EGFRvIII/PTEN were prepared as described<sup>12</sup>. The LIVE/DEAD® Viability/Cytotoxicity Kit (Invitrogen) was used to distinguish live cells from dead cells. For the cell-cycle assay,  $2 \times 10^6$  cells were collected and washed with PBS. DNA content was determined through staining with 50  $\mu\text{g}/\text{mL}$  Propidium Iodide (Sigma) for L1210 cells or BrdU kit (R&D Systems) for U87 EGFRvIII/PTEN cells. Data were acquired on 4 and 5-laser LSRII cytometers (BD Biosciences) and analyzed as previously described<sup>13</sup>.

### **3.2.5. Betabox radioassay**

Each RIMChip assay relies on the use of a pipettor for fluidic control. To replace a solution in microchannels, we always flow a solution from inlets and remove the excess at the outlets using a 100  $\mu\text{l}$  pipettor. For adherent cells, the cells were prepared with fibronectin surface coating. Immediately before cell loading, the outlets were drained of solution. Cells at a concentration of  $3 \times 10^6$  were injected into the microchip from inlets by pressing a pipettor for 5 sec to sufficiently cover all microchannels with cells. Then the outlets were refilled with cell culture medium to prevent the connected microchannels dried up owing to evaporation during incubation in a CO<sub>2</sub> incubator at 37 °C for 4 h. After

incubation, the microchannels were flushed 2× with flowing ~20 µl PBS using the same pipettor, each time for 30 sec, to flush out any residual glucose. About 10 µl  $^{18}\text{F}$ -FDG or  $^{18}\text{F}$ -FAC in PBS was loaded into the microchannels by pressing the pipettor for 15 sec. The whole microchip was then incubated for 30 min in a  $\text{CO}_2$  incubator at 37 °C. It was then flushed 2× with flowing ~20 µl PBS using the same pipettor. The cells in the microchip were then imaged by the beta-box.

For on-chip treatment of cells, we introduced the cells onto the RIMChip 4 h prior to the radioassay. 5mM 2-deoxyglucose (2DG), 10 µM gemcitabine, or 5µM erlotinib, in RPMI 1640 or DMEM medium supplemented with 10% FBS was then added to the microchannels by pipetting, and incubated with cells for 2 hours or designated periods for kinetic study. Drug molecules were removed from the microchannels using two PBS flushing steps. Immediately following, 1 mCi activity of  $^{18}\text{F}$ -FDG in PBS was introduced into the microchambers. One microchannel was loaded with cells, but not treated with gemcitabine. This provided a control assay. The signal from this control was converted into activity/cell, and then used for normalization of the similarly converted signal from the drug-treated cells.

The imaging acquisition time depends on the activity of radioactive probe used for radioassay, with other experimental conditions set. We used 1mCi activity of  $^{18}\text{F}$ -FDG for tests on both adherent and suspended cells, with a fixed incubation time of 30 min. The imaging acquisition time was set for 5 min. We also explored lowering the dosage of  $^{18}\text{F}$ -FAC to 10 µCi/ml for suspended cells, and using an acquisition time of 10 min. Even with such low activity, the radioassay on our platform is still able to differentiate leukemic lines L1210 and its dCK knockdown line.

### 3.2.6. Off-chip radioassay

In parallel with betabox radioassay, off-chip radioassays were performed for each cell sample. Liposarcoma cells were detached from a Petri dish and transferred to a 12 well plate, with each well containing  $\sim 10^4$  cells. The poly-D-lysine coated plates were then placed in a CO<sub>2</sub> incubator at 37 °C for 4 h to allow for cell attachment to well plate bottom. 10  $\mu$ Ci <sup>18</sup>F-FDG or <sup>18</sup>F-FAC was added to each well, followed by 30 minute incubation. Subsequently each well was washed by PBS twice. The cells were then lysed, and the cell lysates were transferred to plastic vials. The radioactivity of each cell sample was measured using a well-type  $\gamma$ -counter (1480 Wizard 3; Perkin Elmer).

### 3.2.7. Phosphoprotein assay

Confluent Petri dishes containing  $5 \times 10^6$  cells were prepared. Lysis buffer (Cell Signaling) with protease inhibitor (Roche) and phosphatase inhibitor (Sigma), was prepared according to the manufacturer's instructions. Following cell lysis, protein concentrations of cell lysates were quantified with a BCA kit (Pierce). A panel of phosphoproteins from the lysates were assayed using a multiplex antibody array<sup>14</sup> and sandwich-type enzyme-linked immunoassays (ELISAs). All proteins in the panel were measured simultaneously from each sample.

### 3.2.8. Data processing

The radioimage was segmented into 20 rectangular regions of interest (ROIs), each of which overlaps a cell chamber and contains > 95% of the beta-particle counts from that

cell chamber. Beta-particle counts of each ROI were quantitated by a custom-written MATLAB program written. The background level was defined from the averaged beta-particle counts from 4 ROIs that covered the 4 cell capture chambers in a microchannel that was not loaded with any cells. For facilitation of cell counting, we stained cells with nuclear dye Hoechst 33342 to visualize each cell under a fluorescence microscope. A script written in ImageJ was used to automate cell counting. Radioactivity of each ROI was normalized by its cell number, and statistics for a given assay condition were calculated from the 4 repeat assays within a given microchannel. We limited comparisons of absolute beta-particle counting results across different experimental conditions to only those assays that were executed on the same RIMChip. To compare the results between RIMChips, we choose one of five microchannels in each RIMChip, and repeat the same experiment across all RIMChips. The radioactivity of other microchannels was normalized to that of the reference microchannel. This meant that we did not need to account for the changing radioactivity from the  $^{18}\text{F}$ -labeled radiopharmaceutical imaging probe.

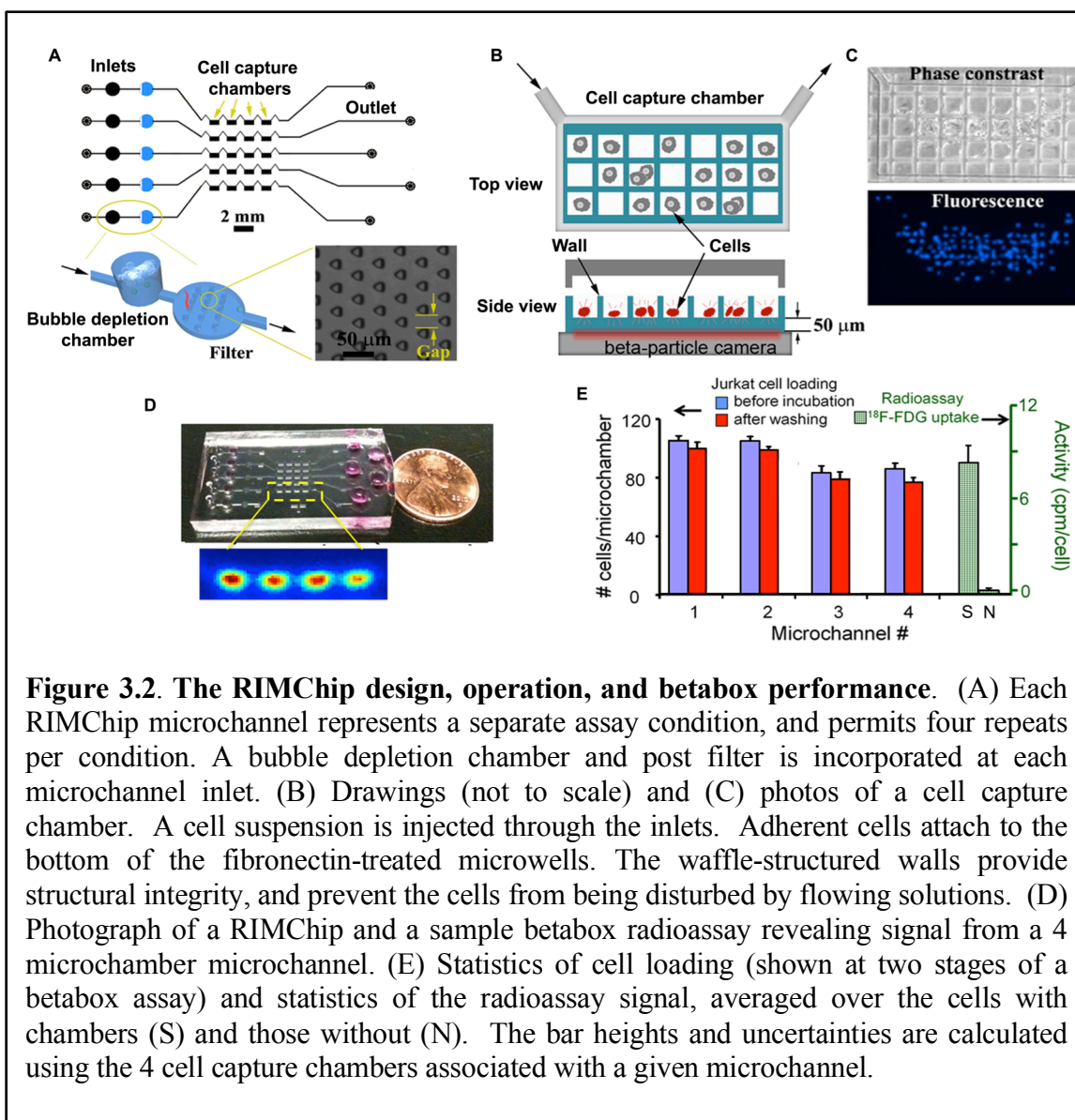
### **3.3. Results**

#### **3.3.1. Design of RIMChip and cell loading**

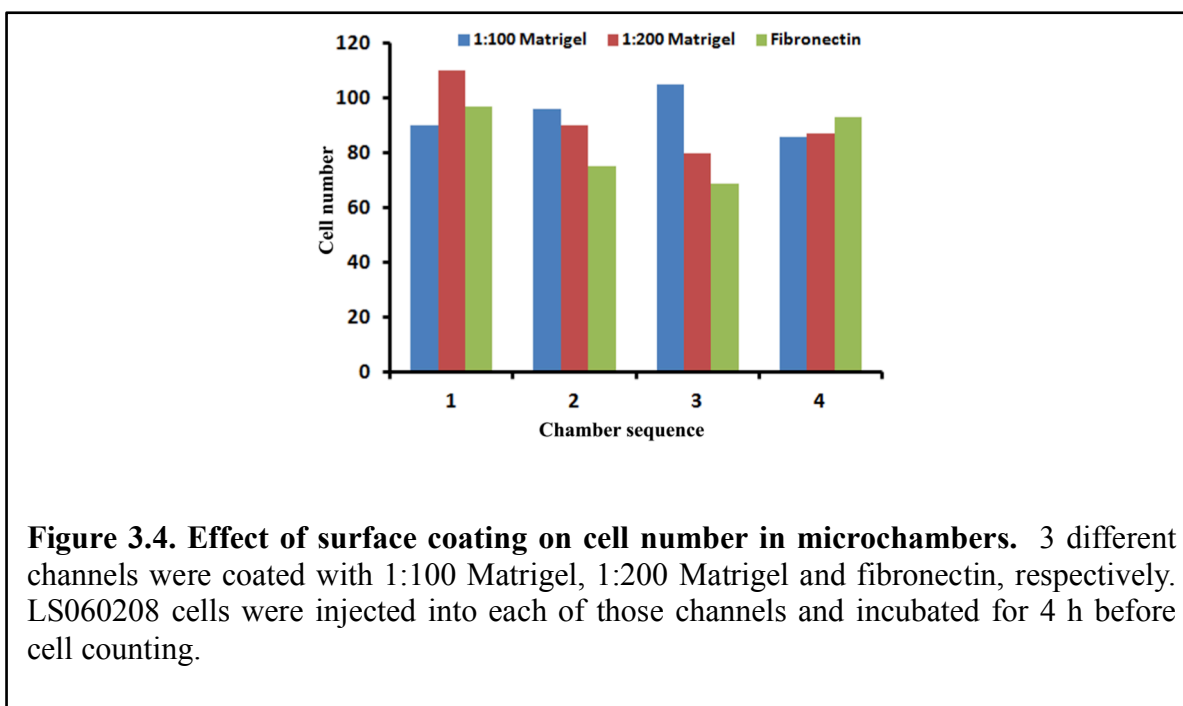
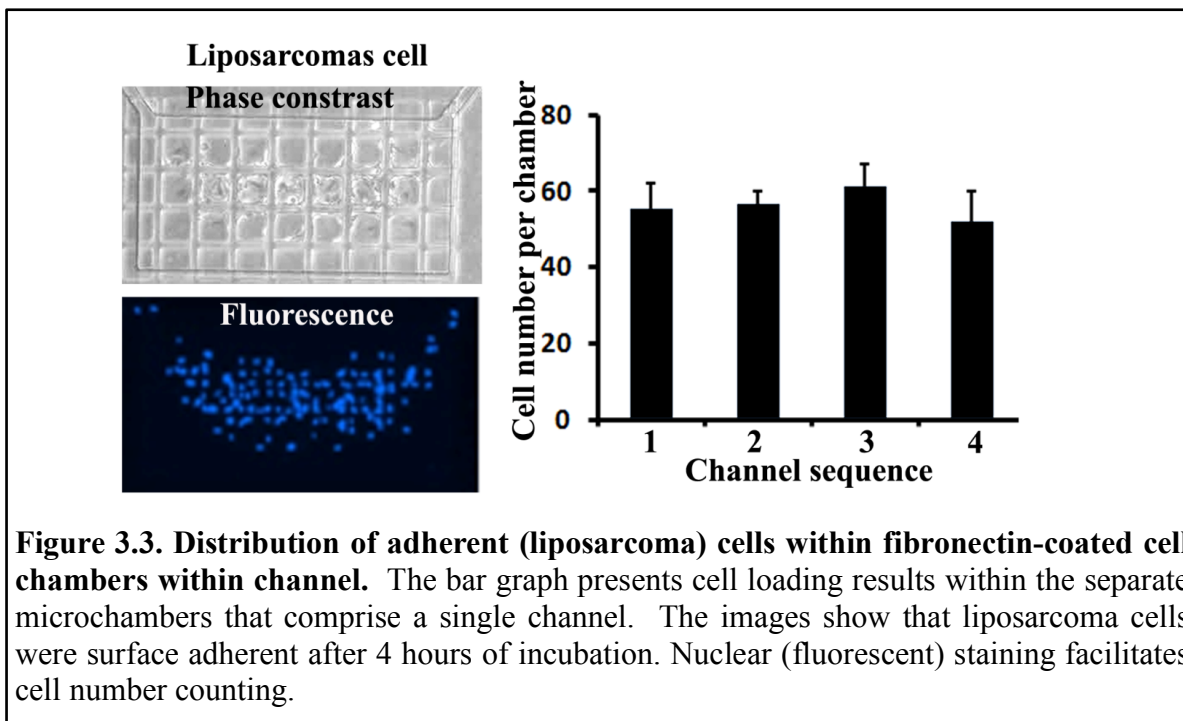
Each RIMChip (**Fig. 3.2.**) permits 4 repeats of 5 independent assays. Each assay microchannel inlet contains a bubble depletion chamber and a debris-trapping filter (**Fig. 3.1., Fig. 3.2. A and B**). These permit the use of standard micropipetting for cell and reagent introduction. The 50  $\mu\text{m}$  separation between the cell capture chamber floors and the camera yields an 11-fold increase in signal level relative to previous designs<sup>2</sup>, which used a microscope cover slip as the chamber floor. Fibronectin coating of the

microchannel surfaces promoted attachment and spreading of the adherent cells (**Fig. 3.3.**), but did not influence the uniformity of cell loading or the [ $^{18}\text{F}$ ]FDG uptake (**Fig. 3.3. and Fig. 3.4.**). Suspension cells were found to attach to the untreated hydrophobic PDMS surface. (**Fig. 3.5.**)

Cells were counted within each cell capture chamber (**Fig. 3.2.C**), before and after the radioassay, to permit per cell quantitation of the radioassay results. Cell loading and [ $^{18}\text{F}$ ]FDG uptake exhibited ~8% variations across the different cell capture chambers associated with a single microchannel. For T cell assays (**Fig. 3.2.E**), chambers with ~ 70-110 cells exhibited a ~30-fold higher signal than control chambers with zero cells.



**Figure 3.2. The RIMChip design, operation, and betabox performance.** (A) Each RIMChip microchannel represents a separate assay condition, and permits four repeats per condition. A bubble depletion chamber and post filter is incorporated at each microchannel inlet. (B) Drawings (not to scale) and (C) photos of a cell capture chamber. A cell suspension is injected through the inlets. Adherent cells attach to the bottom of the fibronectin-treated microwells. The waffle-structured walls provide structural integrity, and prevent the cells from being disturbed by flowing solutions. (D) Photograph of a RIMChip and a sample betabox radioassay revealing signal from a 4 microchamber microchannel. (E) Statistics of cell loading (shown at two stages of a betabox assay) and statistics of the radioassay signal, averaged over the cells with chambers (S) and those without (N). The bar heights and uncertainties are calculated using the 4 cell capture chambers associated with a given microchannel.



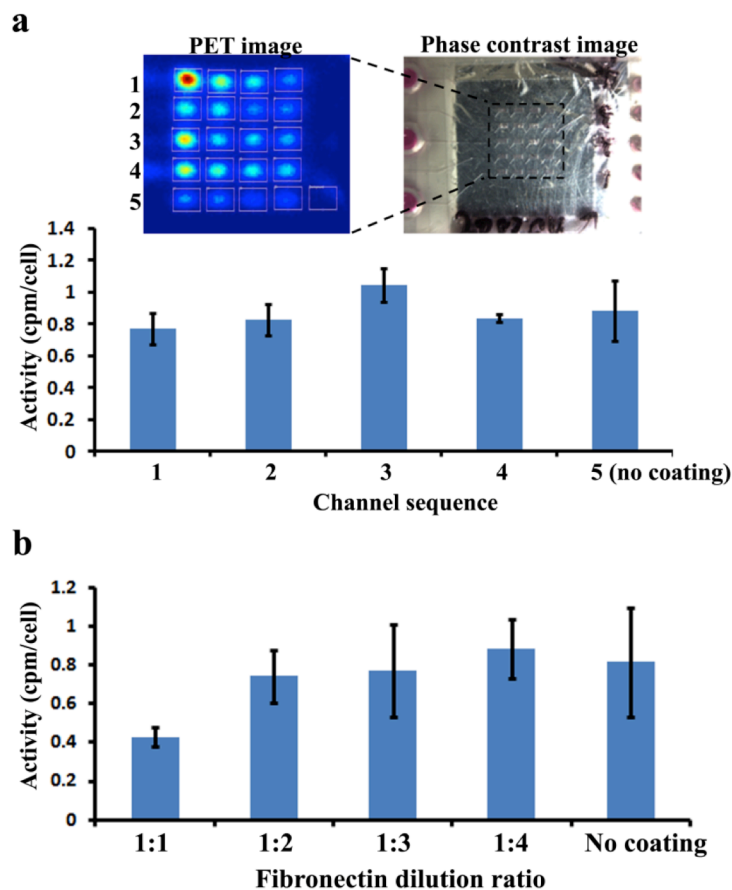
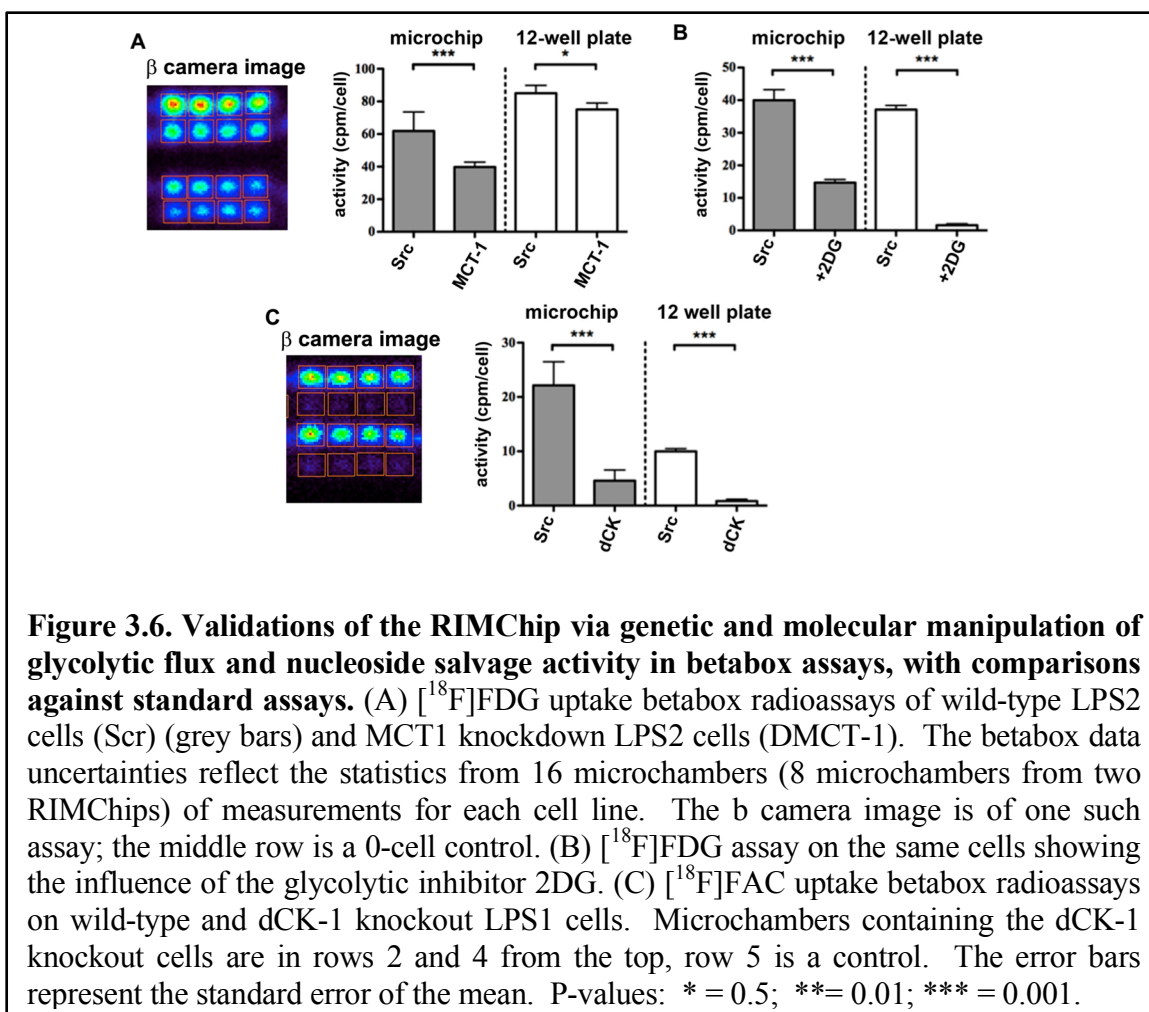


**Figure 3.5. Effect of fibronectin coating on  $^{18}\text{F}$ -FDG uptake by liposarcoma cells.** (a) Channel 1, 2, 3, 4 have been coated with fibronectin for 4 days, 3 day, 2 days, and 1 day, respectively. Channel 5 was not coated with fibronectin. Then cells were loaded to the chambers of each channel and fed with  $^{18}\text{F}$ -FDG following the same procedure as described elsewhere. No significant differences from channel 1 to channel 5 are observed. In channel 5, half of cells were lost after the completion of whole procedure. Cells were not spreading out on an uncoated surface. (b) Effect of fibronectin concentration for coating on uptake of  $^{18}\text{F}$ -FDG. The initial concentration is 1 mg/ml which is diluted 2 times, 3 times and 4 times, respectively. Cells do not demonstrate significant difference with respect to  $^{18}\text{F}$ -FDG uptake except in the cell chambers coated with the highest concentration of fibronectin.

### 3.3.2. Validation of RIMChip

We executed proof-of-principle betabox radioassays in which the glycolytic or nucleoside salvage pathways were genetically or molecularly manipulated in isogenic adherent liposarcoma cell lines (**Fig. 3.6.**). We altered monocarboxylate transporter 1 (MCT-1) levels via stable expression of shRNA, and examined the resulting changes in [ $^{18}\text{F}$ ]FDG uptake (**Fig. 3.6.A**). In these cells, MCT-1 enhances glycolytic flux, so knockdown of MCT1 should result in reduction of [ $^{18}\text{F}$ ]FDG uptake. The RIMChip assays detected a 35% relative decrease in [ $^{18}\text{F}$ ]FDG uptake between Scr and DMCT-1 cells. The conventional assays revealed a 12.5% reduction (**Fig. 3.6.A**). Introduction of the glycolytic inhibitor 2-deoxy-glucose (2DG) resulted in a stronger (3-10 fold) repression of [ $^{18}\text{F}$ ]FDG uptake, as recorded in the RIMChip assay and bulk assays, respectively (**Fig. 3.6.B**).

Certain liposarcomas exhibit nucleoside salvage activity, which can be imaged using the nucleoside analog 1-(2'-deoxy-2' [ $^{18}\text{F}$ ]fluoroarabinofuranosyl) cytosine ([ $^{18}\text{F}$ ]FAC)<sup>8</sup>. [ $^{18}\text{F}$ ]FAC is a substrate for enzyme dCK, and so dCK knockdown should exhibit decreased [ $^{18}\text{F}$ ]FAC uptake. The third betabox validation study supported this hypothesis (**Fig. 3.6.C**).



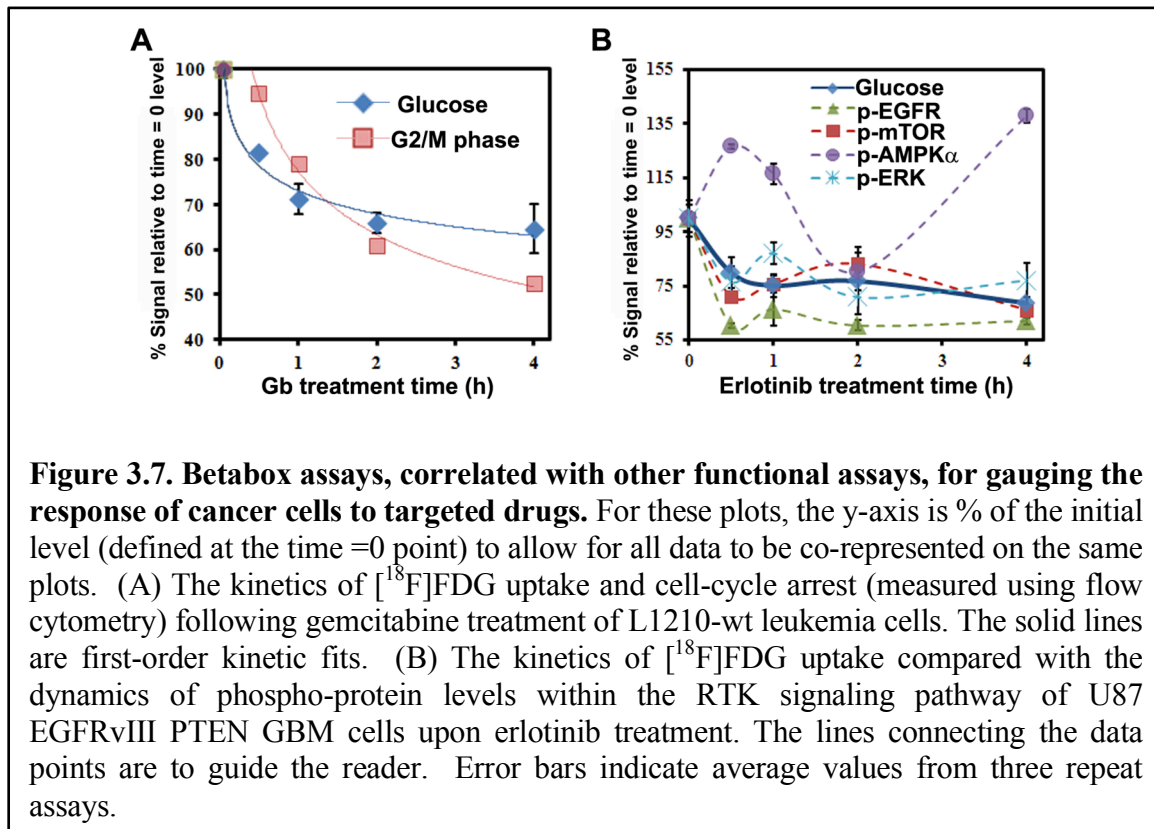
### 3.3.3. Kinetic study of drug response with RIMChip

The betabox was also used for interrogating the kinetics of cellular responses to targeted therapies. All time points in a given kinetics run are imaged simultaneously, for easy comparisons. The influence of gemcitabine on L1210-wt leukemia cells was first studied. Gemcitabine is an anti-cancer pro-drug nucleoside analogue that will impede the cell-cycle in dCK positive tumors<sup>9</sup>. Since glucose metabolism can help fuel the cell-cycle, we reasoned that gemcitabine treatment could influence both [<sup>18</sup>F]FDG uptake and the cell-cycle. Indeed [<sup>18</sup>F]FDG uptake decreases upon cell exposure to gemcitabine, with first-

order kinetics and a half-life ( $\tau_{1/2}$ ) of ~30 minutes cell-cycle arrest exhibits similar kinetics ( $\tau_{1/2}$  ~50 minutes), and lags about 25 minutes behind changes in [ $^{18}\text{F}$ ]FDG uptake. (**Fig. 3.7.A**).

A second class of targeted drugs is aimed at blocking growth factor signaling of receptor tyrosine kinases (RTKs). For example, the ATP-competitive EGFR tyrosine kinase inhibitor erlotinib blocks wild-type and mutant EGFR (EGFRvIII) signaling, inhibiting the phosphorylation of kinases that represent downstream effectors of EGFR<sup>15,16</sup> and thus inhibiting the growth of PTEN-expressing glioblastomas<sup>12</sup>. An activated growth factor signaling pathway implies energy flux through that pathway, so we reasoned that inhibiting that pathway would likely reduce cellular glucose consumption. Thus, we treated EGFRvIII and PTEN-expressing model glioblastoma multiforme (GBM) cell lines with erlotinib, and measured [ $^{18}\text{F}$ ]FDG uptake kinetics, plus the levels of a panel of phosphoproteins that are downstream effectors of EGFR (**Fig. 3.7.B** and **Fig. 3.8**). The full panel of assayed proteins is provided as **Table 3.1**. Again, [ $^{18}\text{F}$ ]FDG uptake drops sharply within 30 min, but the kinetics yield behavior reminiscent of a damped oscillator. Interestingly, this oscillatory behavior is reflected in the changing levels of the assayed phosphoproteins. The protein phosphorylated-AMP activated protein kinase (p-Ampk $\alpha$ ) functions as an energy regulator within the cell<sup>17</sup>. Its level appears to initially oscillate out of phase with [ $^{18}\text{F}$ ]FDG uptake, implying a compensatory mechanism for loss of glucose consumption. The levels of p-EGFR, p-Erk and p-mTOR oscillate mostly in phase with each other, and are partially synchronized with changes in [ $^{18}\text{F}$ ]FDG uptake. The amplitude of the changing levels of a given phosphoprotein may reflect its proximity to EGFR in the RTK signaling pathway. For example, p-EGFR itself exhibits the largest

amplitude response, with p-mTOR exhibiting the weakest response. Over the course of the 4-hour drug treatment window, the cell-cycle was relatively unaffected.



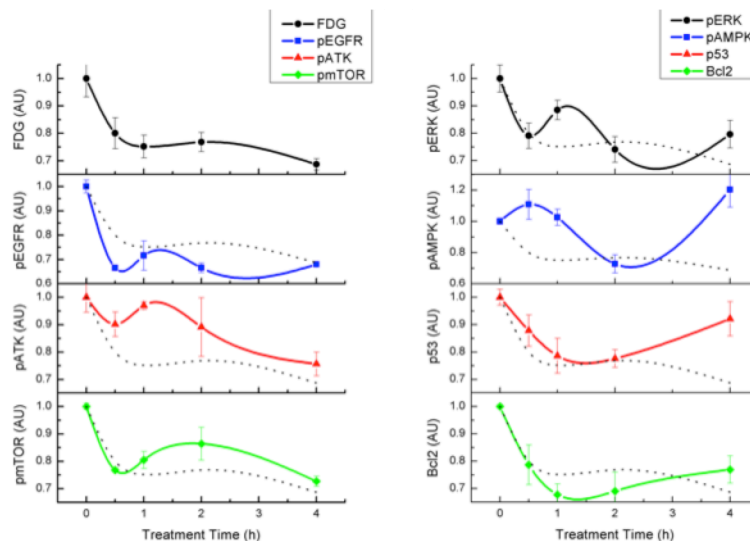


**Figure 3.8.** The kinetics of glucose consumption rate and protein level upon Erlotinib treatment. Each protein is measured and converted to the percentage of the measured level at time 0. Glucose consumption rate has been calculated from  $^{18}\text{F}$ -FDG uptake rate. Error bars indicate fluctuations of three repeats.

**Table 3.1.** List of antibodies used for GBM cell proteomic assay

DNA label	Antibody (ventor: clone)	Source
<b>D</b>	mouse anti-hu phospho-EGFR	R&D Y1068
	biotin-labeled goat anti-hu EGFR	R&D BAF231
<b>E</b>	anti-hu phospho-Ampka kit	R&D DYC 3528
<b>F</b>	anti-hu p53 kit	R&D DYC 1746
<b>G</b>	anti-hu Bcl2 kit	R&D DYC 827B
<b>I</b>	anti-hu phospho-mTOR kit	R&D DYC 1665
<b>K</b>	anti-hu phospho-ERK kit	R&D DYC 1018B
<b>L</b>	anti-hu phospho-Akt1 kit	R&D DYC 2289

### 3.4. Discussions

The comparisons of **Fig. 3.6.** between the betabox assays and the 12-well plate (bulk) assays reveal qualitative, but not fully quantitative agreement between the two approaches. A concern might be that since the RIMChip assays a relatively small number of cells, the corresponding statistical spread of results would be significantly larger than for the bulk assays. However, this spread, which should scale as the square root of the numbers of cells, is not large. For the comparisons of **Fig 3.6.**, 4 microchannels  $\times$  4 microchambers per channel  $\times$  100 cells per microchamber yields a 2.5% error, relative to an expected  $\sim$ 0.5% error for a ( $\sim$ 50,000 cells) bulk assay. Cell counting errors for the RIMChip assays may add a few additional percent, as will the experimental errors in manipulating the cells for the bulk assay. Small variations in the 50  $\mu$ m thick PDMS membrane separating the cells from the camera can also contribute a few percent error. However, given that the two techniques have independent sources of error, and that the RIMChip assays for  $\sim$ 50-fold fewer cell numbers, the agreement between the two techniques is good. There is a flow cytometry-based assay that utilizes a fluorophore-labeled [ $^{18}$ F]FDG analogue, but recent literature<sup>18</sup> has called into question the validity of that assay, and so we did not compare against it here.

The kinetic responses recorded in **Fig. 3.7.** reveal that the [ $^{18}$ F]FDG RIMChip assay provides a rapid ( $<$  1 hour) tool for detecting the response of small cell numbers to a therapy. However, the assays also reveal different response kinetics for the different cell lines and drugs. An exact resolution of such responses can be accomplished by either capturing the dynamic trajectories of individual cells<sup>19</sup>, or the fluctuations of the functional proteins at the single-cell level<sup>20</sup>. Obviously, the RIMChip assay does not resolve such

trajectories of fluctuations, but the cited literature can provide some insight into the observed responses. For example, the first-order relaxation kinetics observed for the response of the L1210 leukemia cells to gemcitabine exposure is consistent with a transition between two distinct, steady state descriptions of those cells. An alternative explanation, which we can rule out by our observations, is that gemcitabine exposure killed a fraction of the cells. No dead cells were detected during the course of the experiment. The oscillatory dynamics observed for the erlotinib treated GBM cells imply that there are competing networks that influence the kinetics. The overall result may be the same-i.e., the cells are switching between two states, but that is not as clear from our data. Again, however, no dead cells were detected during the course of the experiments.

### 3.5. Conclusions

The betabox platform, comprised of a microfluidic chip (the RIMChip) mated to a beta-particle imaging camera, enables robust, user-friendly execution of sensitive and quantitative cell-based radioassays. Each radioassay requires ~100 cells. Betabox radioassays provide a useful and rapid screening platform for investigating the response of various cell lines to mechanistically distinct, targeted drugs. The betabox platform provides a rapid screening tool for a variety of drug/cell line combinations, as well as a powerful tool for mechanistic investigations.

### 3.6. References

1. Czernin, J. & Phelps, M. E. Positron emission tomography scanning: current and future applications. *Annu. Rev. Med.* **53**, 89–112 (2002).
2. Vu, N. T. *et al.* A Camera Integrated with a Microfluidic Chip for Radioassays Based on

- Real-Time Imaging of Glycolysis in Small Cell Populations. *J Nucl Med* **52**, 815–821 (2011).
3. Dooraghi, A. A. *et al.* Betabox: a beta-particle imaging system based on a position sensitive avalanche photodiode. *Phys Med Biol* **58**, 3739–3753 (2013).
  4. Fang, C. *et al.* Integrated Microfluidic and Imaging Platform for a Kinase Activity Radioassay to Analyze Minute Patient Cancer Samples. *Cancer Res* **70**, 8299–8308 (2010).
  5. Usova, E., Maltseva, T., Földesi, A., Chattopadhyaya, J. & Eriksson, S. Human deoxycytidine kinase as a deoxyribonucleoside phosphorylase. *Journal of Molecular Biology* **344**, 1347–1358 (2004).
  6. Radu, C. G. *et al.* Molecular imaging of lymphoid organs and immune activation by positron emission tomography with a new [18F]-labeled 2'-deoxycytidine analog. *Nature Medicine* **14**, 783–788 (2008).
  7. Shipley, L. A. *et al.* Metabolism and disposition of gemcitabine, and oncolytic deoxycytidine analog, in mice, rats, and dogs. *Drug Metab. Dispos.* **20**, 849–855 (1992).
  8. Braas, D. *et al.* Metabolomics strategy reveals subpopulation of liposarcomas sensitive to gemcitabine treatment. *Cancer Discov* **2**, 1109–1117 (2012).
  9. Laing, R. E. *et al.* Noninvasive prediction of tumor responses to gemcitabine using positron emission tomography. *P Natl Acad Sci USA* **106**, 2847–2852 (2009).
  10. Jordheim, L. P. *et al.* Characterization of a gemcitabine-resistant murine leukemic cell line: reversion of in vitro resistance by a mononucleotide prodrug. *Clin Cancer Res* **10**, 5614–5621 (2004).
  11. Owens, J. K., Shewach, D. S., Ullman, B. & Mitchell, B. S. Resistance to 1-beta-D-arabinofuranosylcytosine in human T-lymphoblasts mediated by mutations within the deoxycytidine kinase gene. *Cancer Res* **52**, 2389–2393 (1992).
  12. Mellinghoff, I. K. *et al.* Molecular determinants of the response of glioblastomas to EGFR kinase inhibitors. *N Engl J Med* **353**, 2012–2024 (2005).
  13. Fenton, T. R. *et al.* Resistance to EGF receptor inhibitors in glioblastoma mediated by phosphorylation of the PTEN tumor suppressor at tyrosine 240. *P Natl Acad Sci USA* **109**, 14164–14169 (2012).
  14. Bailey, R. C., Kwong, G. A., Radu, C. G., Witte, O. N. & Heath, J. R. DNA-encoded antibody libraries: a unified platform for multiplexed cell sorting and detection of genes and proteins. *J. Am. Chem. Soc.* **129**, 1959–1967 (2007).
  15. Huang, P. H. *et al.* Quantitative analysis of EGFRvIII cellular signaling networks reveals a combinatorial therapeutic strategy for glioblastoma. *P Natl Acad Sci USA* **104**, 12867–

- 12872 (2007).
16. Shi, Q. *et al.* Single-cell proteomic chip for profiling intracellular signaling pathways in single tumor cells. *P Natl Acad Sci USA* **109**, 419–424 (2012).
  17. Inoki, K., Kim, J. & Guan, K.-L. AMPK and mTOR in Cellular Energy Homeostasis and Drug Targets. *Annu. Rev. Pharmacol. Toxicol.* **52**, 381–400 (2012).
  18. Tseng, J.-C., Wang, Y., Banerjee, P. & Kung, A. L. Incongruity of imaging using fluorescent 2-DG conjugates compared to 18F-FDG in preclinical cancer models. *Mol Imaging Biol* **14**, 553–560 (2012).
  19. Gascoigne, K. E. & Taylor, S. S. Cancer cells display profound intra- and interline variation following prolonged exposure to antimitotic drugs. *Cancer Cell* **14**, 111–122 (2008).
  20. Wei, W. *et al.* Hypoxia induces a phase transition within a kinase signaling network in cancer cells. *P Natl Acad Sci USA* **110**, E1352–60 (2013).